

Effect of Water and Aerosols Absorption on Laser Beam Propagation in Moist Atmosphere at Eye-Safe Wavelength of 1.57 μm

Yoshito Shuto

Ofra Project, Iruma City, Japan

Email address:

ofra@tuba.ocn.ne.jp

To cite this article:

Yoshito Shuto. Effect of Water and Aerosols Absorption on Laser Beam Propagation in Moist Atmosphere at Eye-Safe Wavelength of 1.57 μm . *Journal of Electrical and Electronic Engineering*. Vol. 11, No. 1, 2023, pp. 15-22. doi: 10.11648/j.jeeec.20231101.12

Received: January 4, 2023; **Accepted:** January 25, 2023; **Published:** February 6, 2023

Abstract: To realize optical wireless power transmission, atmospheric propagation of eye-safe wavelength (1.57 μm) laser beams was theoretically investigated. Laser beams are affected by the presence of water vapor and aerosols which absorb and scatter the laser energy. The scattering coefficients of water molecules and aerosols were estimated to be about 6.3×10^{-7} and $5.6 \times 10^{-5} \text{ m}^{-1}$, respectively, at wavelength (λ_0) of 1.57 μm . Furthermore, the absorption coefficients of moist air at 30% relative humidity and aerosols were estimated to be about 6.16×10^{-3} and $2.52 \times 10^{-5} \text{ m}^{-1}$, respectively, at $\lambda_0 = 1.57\mu\text{m}$. Then simulation of laser beam propagation in the moist atmosphere at $\lambda_0 = 1.57\mu\text{m}$ was performed using these coefficients. Under the condition of no wind, the beam intensity decreases rapidly with increasing the length z and the rate of decrease slows down as the beam radius (ω) increases. When z_h is defined as the z where the normalized intensity is halved, the $z_h (= 25 \text{ m})$ at $\omega = 20 \text{ mm}$ when input power $P = 10 \text{ W}$ is about three times longer than that ($= 8 \text{ m}$) when $P = 100 \text{ W}$. This result indicates that the thermal distortion of laser beams due to accumulated heat around the z axis becomes more conspicuous as the optical power increases. The effect of this thermal beam distortion can be weakened when the laser beam is subject to crosswinds. Under the condition of gentle uniform wind with wind velocity $v = 5 \text{ m/s}$, propagation of laser beams with $\omega = 20 \text{ mm}$ was studied when $P = 100 \text{ W}$. The $z_h (= 105 \text{ m})$ when $v = 5 \text{ m/s}$ is about 13 times longer than that ($= 8 \text{ m}$) when $v = 0 \text{ m/s}$. Thus, under conditions of $v = 5 \text{ m/s}$ and 30% relative humidity, laser beams with $P = 100 \text{ W}$ and $\omega = 20 \text{ mm}$ can propagate over 100 m without damaging the initial beam shape at $\lambda_0 = 1.57\mu\text{m}$.

Keywords: Laser Beam Propagation, Moist Atmosphere, Aerosol, Optical Wireless Power Transmission, Eye-Safe Wavelength

1. Introduction

Wireless power transmission (WPT) is an important technology to transmit energy remotely from a power source to an electrical apparatus [1]. WPT technology relies on electromagnetic radiation, such as microwaves and/or optical beams, to enable long-distance energy transfer.

As for microwave WPT (MWPT), a large-sized phased-array antenna is necessary for increasing the directivity and transmission efficiency owing to large diffraction effect of microwaves. In addition, high power electromagnetic radiation results in the serious issue of electromagnetic interference (EMI) to the target apparatus and surrounding electrical devices.

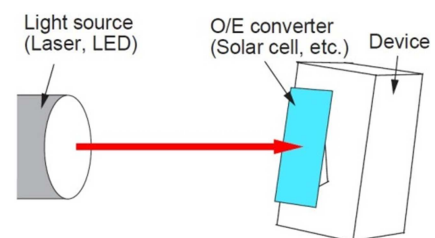


Figure 1. Basic concept of OWPT.

On the other hand, optical WPT (OWPT) is the only WPT technology with the advantages of long transmission distance, high directivity, and no EMI noise [2]. Even compared with MWPT, OWPT has the potential to maintain high efficiency

over long transmission distances due to small diffraction effect of light. Figure 1 shows basic concept of OWPT.

The light source (laser or light emitting diode) and the O/E converter (solar cell, etc.) are basic devices of OWPT. Solar cell has advantages of high O/E conversion efficiency and thin thickness.

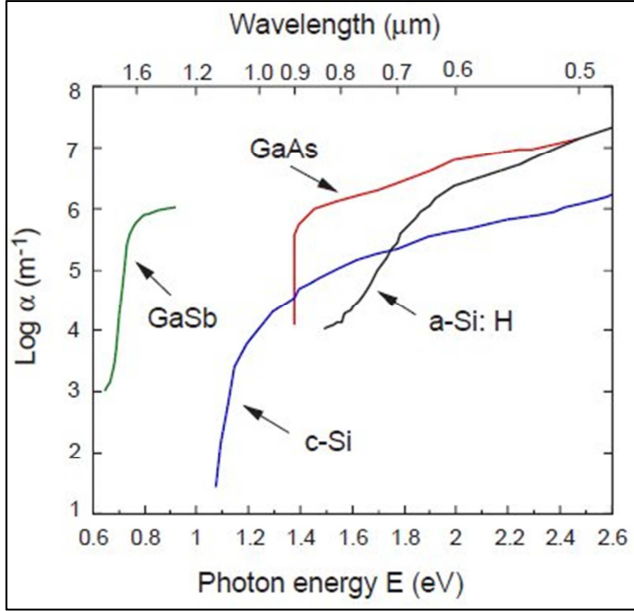


Figure 2. Absorption spectra of commercially available solar cells and semiconductors.

Figure 2 shows the absorption spectra of several commercially available solar cells and semiconductors. As shown in Figure 2, GaAs and hydrogenated amorphous silicon (a-Si:H) exhibit large absorption coefficients (α s) of $> 10^6 \text{ m}^{-1}$ at the wavelength of < 0.8 and $< 0.65 \mu\text{m}$, respectively. These α s are larger than that of crystalline silicon (c-Si). On the other hand, GaSb exhibits large α of $> 10^5 \text{ m}^{-1}$ at the wavelength range from 1.4 to $1.7 \mu\text{m}$.

Miyamoto and coworkers reported vertical cavity surface emitting laser (VCSEL) array and/or light emitting diode (LED) based OWPT systems using c-Si and/or GaAs solar cells [2-6]. In their systems, operation wavelengths of light sources were 0.975/0.850 and/or 0.810 μm .

Increasing the laser power raises the issue of safety to the human body. Laser safety is governed by the IEC 60825-1 standard [7]. This standard gives safety limits for exposure to laser light. Safety limits vary by wavelength and duration of exposure. Generally speaking, the longer the wavelength and the shorter the irradiation time, the higher the safety [8].

Sahai and Graham proposed laser diode array based OWPT systems using a commercially available GaSb semiconductor as an O/E converter [9]. In their system, a commercially available multi-mode InGaAsP/InP edge-emitting laser diode array was used as a light source and the oscillation wavelength of the semiconductor laser was set to 1.40 μm considering laser safety.

Furthermore, Mukherjee and coworkers reported laser power transfer experiments across a distance of 30 m at an

eye-safe wavelength of 1.55 μm [10]. In their system, a diode pumped high power fiber laser and lattice-matched InGaAsP/InP were used as a light source and O/E converter. A maximum O/E conversion efficiency of about 45% was achieved at an incident laser power density of about 1 kW/m^2 and above [10-12].

High-power erbium (Er)-ytterbium (Yb) co-doped fiber lasers operating in the eye-safe wavelength regime around ~ 1.5 - $1.6 \mu\text{m}$ have been investigated by several research institutes [13-23]. A high output power of $\geq 100 \text{ W}$ in the continuous-wave (CW) laser operation at $\lambda_0 \approx 1.57 \mu\text{m}$ using cladding-pumped Er-Yb-co-doped large-core fibers [17, 21, 23] has been reported.

In order to transfer high-power laser beam to a distant O/E converter, the laser beam must propagate through the moist atmosphere. Atmospheric propagation of laser beams at eye-safe wavelength of 1.57 μm is affected by the presence of water molecules and aerosols which absorb and/or scatter the laser energy.

In this article, we investigated the effect of water molecules and aerosol on high-power laser beam propagation in the moist atmosphere at $\lambda_0 = 1.57 \mu\text{m}$.

2. Extinction Coefficients of Water and Aerosols

The relationship between the extinction coefficient (α_{ext}), the absorption coefficient (α_{abs}), and the scattering coefficient (α_{sca}) is given by

$$\alpha_{\text{ext}} = \alpha_{\text{abs}} + \alpha_{\text{sca}} \quad (1)$$

2.1. Scattering Coefficients

Scattering of laser beams in the atmosphere is caused by gaseous molecules and aerosols. The molecular scattering is appreciable only for the shorter visible wavelengths while beyond about $1 \mu\text{m}$ the scattering can be attributed to the atmospheric aerosols [24].

The α_{sca} value of water molecules in the atmosphere was 6.0 - $6.5 \times 10^{-7} \text{ m}^{-1}$ at $\lambda_0 = 1.57 \mu\text{m}$ [25].

On the other hand, the α_{sca} values of aerosols vary greatly depending on weather conditions, especially the absolute or the relative humidity, and seasons [26]. If the aerosol size distribution is known, as well as the effective index of refraction of the aerosol, the α_{sca} can be calculated using the Mie scattering theory [27-29].

Barnhardt and Streete estimated the α_{sca} values at various relative humidity using a two-component composite of continental and maritime size distributions of aerosols [24]. Their estimated α_{sca} value for a 2.5:1.0 continental: maritime mixing for 50% relative humidity was about $5.6 \times 10^{-5} \text{ m}^{-1}$ at $\lambda_0 = 1.57 \mu\text{m}$ [24].

McClatchey and Selby reported aerosol scattering data for both clear (23-km visibility) and hazy (5-km visibility) conditions [30]. The α_{sca} value for clear atmosphere condition was about $6.2 \times 10^{-5} \text{ m}^{-1}$ at $\lambda_0 = 1.57 \mu\text{m}$ [30].

Estimated α_{sca} value ($5.6 \times 10^{-5} \text{ m}^{-1}$) of aerosols is close to that (about $6.2 \times 10^{-5} \text{ m}^{-1}$) for clear condition.

2.2. Absorption Coefficients

2.2.1. Water

In the atmospheric absorption at $\lambda_0 = 1.57\mu\text{m}$, the dominant molecular absorber is water vapor.

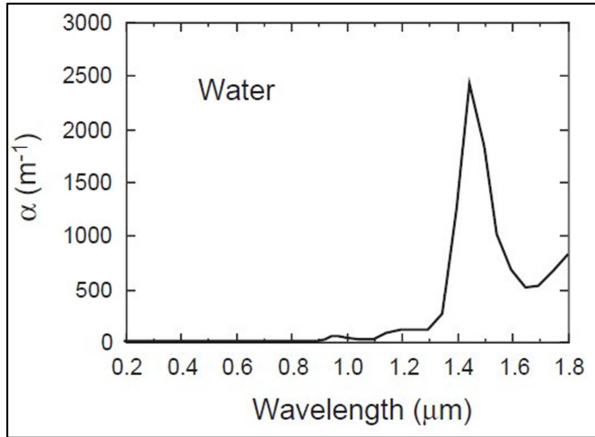


Figure 3. Absorption coefficients of water.

Figure 3 shows the absorption coefficients of water at 293 K for the spectral region from 0.2 to $1.8\mu\text{m}$ [31, 32].

As shown in Figure 3, water molecules exhibit a strong absorption peak at $1.45\mu\text{m}$ and an absorption coefficient α_w of liquid water is about $8.0 \times 10^2 \text{ m}^{-1}$ at $\lambda_0 = 1.57\mu\text{m}$ [31].

On the other hand, the relationship between the water vapor density ρ_v (unit: kg m^{-3}) at 300 K and relative humidity h is given by the following equation [33].

$$\rho_v = 0.02557 \cdot h \quad (2)$$

When relative humidity h is 30%, the ρ_v value at 300 K was estimated to be about $7.67 \times 10^{-3} \text{ kg m}^{-3}$ by using Eq. (2).

By comparing this water vapor density with the density ρ ($= 996.62 \text{ kg m}^{-3}$ [34]) of the saturated water at 300 K, the water content c_w per 1 m^3 of moist air at 30% relative humidity was estimated to be about 7.7×10^{-6} .

By using c_w and α_w , the absorption coefficient α_{abs} of moist air at 30% relative humidity is given by

$$\alpha_{\text{abs}} = c_w \cdot \alpha_w \quad (3)$$

By using Eq. (3), the α_{abs} of moist air at 30% relative humidity was estimated to be $6.16 \times 10^{-3} \text{ m}^{-1}$ at $\lambda_0 = 1.57\mu\text{m}$.

2.2.2. Aerosols

Aerosol light absorption in the atmosphere is dominated by black carbon (BC) with additional significant contributions from brown carbon (BrC) and mineral dust (MD) [35]. The α_{abs} values of aerosols have been estimated at the visible and near-visible wavelengths [35-44].

In this subsection, the α_{abs} value of aerosols (BC, BrC, and MD) at $\lambda_0 = 1.57\mu\text{m}$ were estimated as follows.

Parameters related to aerosol absorption are shown in Table 1.

Table 1. Parameters of aerosol absorption.

Parameter	Unit	BC	BrC	MD
k_{VIS}	-	0.79 [36]	0.27 [41]	0.0027 [44]
β_{VIS}	10^6 m^{-1}	18.1	6.2	0.062
β_{NIR}	10^6 m^{-1}	6.3	1.3	0.022
AAC	-	1.0	1.5	1.0
ρ	kg m^{-3}	1,350 [34]	1,350 [34]	1,510 [34]
c	$\mu\text{g m}^{-3}$	~ 5 [45]	~ 2 [46]	~ 18 [47]
α_{NIR}	10^{-5} m^{-1}	2.3	0.19	0.027

In this table, the subscripts VIS and NIR indicate that the physical properties were identified at wavelengths (λ) of 0.55 and $1.57\mu\text{m}$, respectively.

k and β are the imaginary part of the refractive index and the absorption coefficient of an aerosol material.

β_{VIS} is related to k_{VIS} as

$$\beta_{\text{VIS}} = \frac{4\pi k_{\text{VIS}}}{\lambda_{\text{VIS}}}, \quad (4)$$

where $\lambda_{\text{VIS}} = 0.55\mu\text{m}$.

On the other hand, β_{NIR} is related to β_{VIS} as

$$\beta_{\text{NIR}} = \beta_{\text{VIS}} \left(\frac{\lambda_{\text{NIR}}}{\lambda_{\text{VIS}}} \right)^{-AAC}, \quad (5)$$

where $\lambda_{\text{NIR}} = 1.57\mu\text{m}$ and AAC is the absorption Ångström coefficient [48]. AAC close to 1 is expected in spectral regions where the refractive index of the aerosol material has a weak spectral dependence, just like BC [36, 41] and MD, whereas $AAC = 1.5$ is assumed to BrC [41].

By using the mass concentration c , mass density ρ , and β_{NIR} , the absorption coefficient α_{NIR} of the aerosol material is given by

$$\alpha_{\text{NIR}} = \frac{c}{\rho} \beta_{\text{NIR}} \quad (6)$$

As shown in Table 1, the α_{NIR} value of BC is larger than those of BrC and MD. The sum of α_{NIR} values of BC, BrC, and MD is defined as the absorption coefficient α_{abc} of aerosols.

This α_{abs} ($= 2.52 \times 10^{-5} \text{ m}^{-1}$) is smaller than that ($6.16 \times 10^{-3} \text{ m}^{-1}$) of moist air at 30% relative humidity.

McClatchey and Selby reported aerosol absorption data for both clear (23-km visibility) and hazy (5-km visibility) conditions at $\lambda_0 = 1.57\mu\text{m}$ [30]. The α_{abs} values for clear and hazy conditions were about 1.0 and $4.9 \times 10^{-5} \text{ m}^{-1}$, respectively [30]. The α_{abs} ($2.52 \times 10^{-5} \text{ m}^{-1}$) estimated above is between the values of the clear and hazy condition.

Scattering and absorption coefficients of water vapor and aerosols estimated at $\lambda_0 = 1.57\mu\text{m}$ are listed in Table 2.

Table 2. Scattering and absorption coefficients at $1.57\mu\text{m}$.

Parameter	Unit	Water Vapor (30%RH)	Aerosols (BC, BrC, MD)
α_{sca}	10^{-5} m^{-1}	0.063	5.6
α_{abs}	10^{-3} m^{-1}	6.16	0.0252

In the following calculation, the sum ($= 6.19 \times 10^{-3} \text{ m}^{-1}$) of α_{abs} values of water vapor and aerosols was used as the absorption coefficient α_{abs} of the moist atmosphere. On the

other hand, the extinction coefficient $\alpha_{\text{ext}} (= \alpha_{\text{abs}} + \alpha_{\text{sca}})$ was used as α .

3. Simulation of Gaussian Laser Beam Propagation

Propagation of Gaussian laser beams in the moist atmosphere was investigated theoretically.

3.1. Laser Beam Propagation with No Crosswind

In this subsection, for the sake of analysis, we assumed that there is no relative motion (no wind) between the laser beam and the moist air. Laser beam propagates along the z direction at $\lambda_0 = 1.57 \mu\text{m}$.

When laser beams propagate in the moist atmosphere, thermal distortion of laser beams arises because the absorbed laser power in the atmosphere changes the index of refraction and therefore changes the beam intensity itself [49]. A stable state is created by balancing the dissipation of heat due to heat conduction in the xy -plane orthogonal to the traveling z -direction of light and the increase in heat due to absorption of laser power by water vapor and aerosols in the atmosphere.

The steady state solution for an initially collimated Gaussian laser beam propagating through the atmosphere at a point z away from the output end ($z = 0$) of laser was derived as follows: [49, 50].

$$\frac{I(x, y, z)}{I_0} = \exp \left\{ -\alpha z - \frac{x^2 + y^2}{\omega^2} \right\} g(x, y, z, P, \omega) \quad (7)$$

where $I_0 = I(0, 0, 0)$ and ω is the beam radius of the Gaussian laser beam. In this equation, the intensity $I(x, y, z)$ was normalized by dividing by I_0 .

The function g represents the effect of thermal distortion of the laser beam. This function is given by

$$g(x, y, z, P, \omega) = \exp \left\{ \left(\frac{\partial n}{\partial T} \right)^P \left[z + \frac{e^{-\alpha_{\text{abs}} z} - 1}{\alpha_{\text{abs}}} \right] e^{-(x^2 + y^2)/\omega^2} \right\} \quad (8)$$

where $\partial n / \partial T (= -0.92 \times 10^{-6} \text{ K}^{-1})$ [33], $\lambda (= 0.02614 \text{ W m}^{-1} \text{ K}^{-1})$ [34], and $n (= 1.000274)$ are the thermal coefficient of the refractive index, thermal conductivity, and refractive index of the moist atmosphere at 300 K and $\lambda_0 = 1.57 \mu\text{m}$, respectively. P is the initial power of the Gaussian laser beam.

When $x = y = 0$, Eq. (7) can be rewritten as

$$\frac{I(0, 0, z)}{I_0} = \exp \left\{ -\alpha z + \left(\frac{\partial n}{\partial T} \right)^P \left[z + \frac{e^{-\alpha_{\text{abs}} z} - 1}{\alpha_{\text{abs}}} \right] \right\} \quad (9)$$

The normalized intensity distributions of laser beam at $\omega = 10, 20, 30$, and 40 mm were calculated using Eq. (9) when $P = 10$ or 100 W , 30% relative humidity, and $\lambda_0 = 1.57 \mu\text{m}$. The calculated results are shown in Figures 4 and 5.

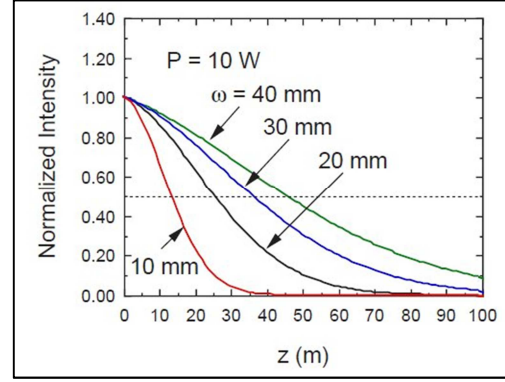


Figure 4. Normalized intensity distributions of laser beams with $P = 10 \text{ W}$ and $\omega = 10, 20, 30$, and 40 mm at 30% relative humidity and $\lambda_0 = 1.57 \mu\text{m}$.

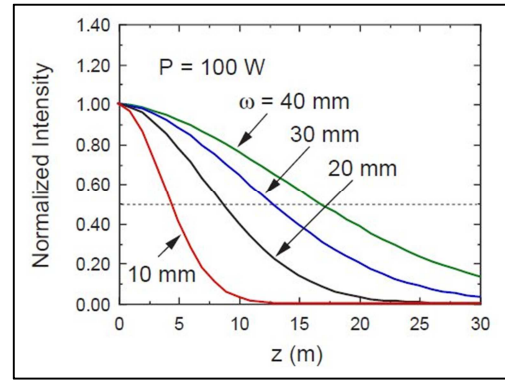


Figure 5. Normalized intensity distributions of laser beams with $P = 100 \text{ W}$ and $\omega = 10, 20, 30$, and 40 mm at 30% relative humidity and $\lambda_0 = 1.57 \mu\text{m}$.

As shown in Figures 4 and 5, the beam intensity decreases rapidly with increasing z and the rate of decrease slows down as ω increases.

Let z_h be the z where the normalized intensity is halved, then the $z_h (= 25 \text{ m})$ at $\omega = 20 \text{ mm}$ when $P = 10 \text{ W}$ is about three times longer than that ($= 8 \text{ m}$) when $P = 100 \text{ W}$.

This result indicates that the thermal distortion of laser beams due to accumulated heat around the z axis becomes more conspicuous as the optical power increases.

The effect of this thermal beam distortion can be weakened when the laser beam is subject to crosswinds [51].

In the following subsection, we described the calculation results of Gaussian laser beam propagation in moist atmosphere with gentle uniform crosswind at $\lambda_0 = 1.57 \mu\text{m}$.

3.2. Laser Beam Propagation with Gentle Uniform Crosswind

When an initially collimated Gaussian laser beam propagates in the moist atmosphere with transverse air flow, thermal distortion of the beam is not symmetrical around the z axis because of the asymmetry introduced by the one-dimensional wind velocity.

For the sake of analysis, we assumed that there is a uniform wind with the velocity v in the x direction.

Taking into account this problem, the steady state solution for the initially Gaussian laser beam was derived by Gebhardt and Smith [52]. The solution is as follows:

$$\frac{I(x,y,z)}{I_0} = \exp\left\{-\alpha z - \frac{x^2+y^2}{\omega^2}\right\} \exp\left\{N\left[2\left(\frac{x}{\omega}\right)e^{-\frac{x^2+y^2}{\omega^2}} + \frac{\sqrt{\pi}}{2}e^{-\frac{y^2}{\omega^2}}\left(1 - 4\frac{y^2}{\omega^2}\right)\left(1 + \operatorname{erf}\left(\frac{x}{\omega}\right)\right)\right]\right\} \equiv e^{-\alpha z} f(x,y,z), \quad (10)$$

where

$$N = \frac{2\left(\frac{\partial n}{\partial T}\right)^P}{\rho C_p n v \pi \omega^3} \left[z + \frac{e^{-\alpha_{abs} z} - 1}{\alpha_{abs}}\right] \quad (11)$$

Here ρ ($= 1176.3 \text{ kg m}^{-3}$ [34]) and C_p ($= 1007 \text{ J kg}^{-1} \text{ K}^{-1}$

[34]) are the density and specific heat of the moist atmosphere at 300 K, respectively. $\operatorname{erf}(x)$ is the error function with respect to x .

For the function f , the following formula holds for all z .

$$\iint f(x,y,z) dx dy = \text{constant} \quad (12)$$

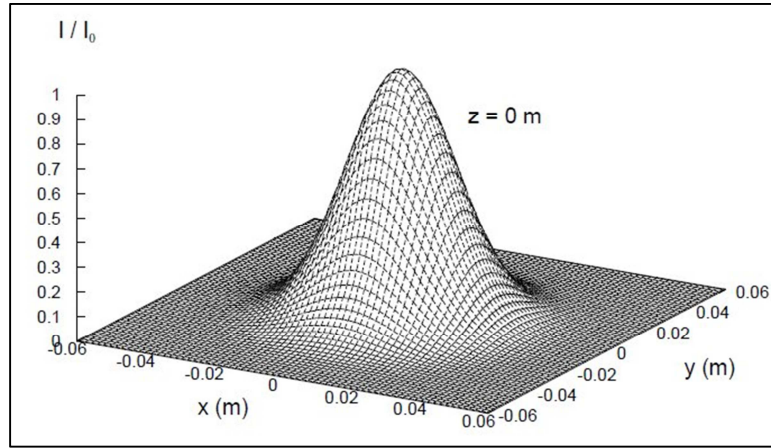


Figure 6. Normalized intensity distribution of laser beam at $z = 0 \text{ m}$ with $v = 5 \text{ m/s}$ and 30% relative humidity.

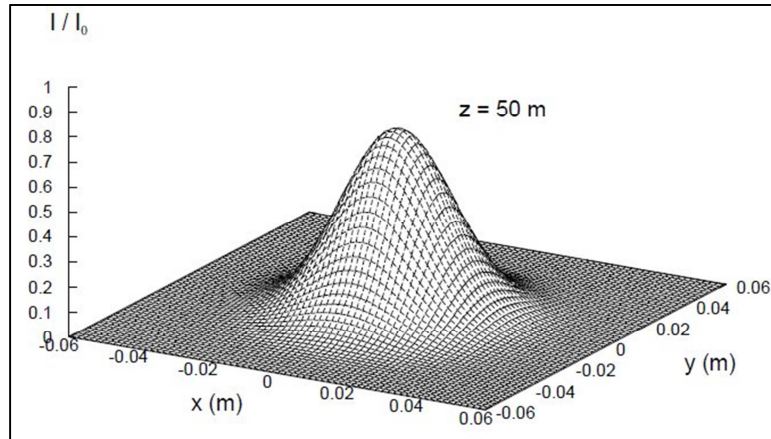


Figure 7. Normalized intensity distribution of laser beam at $z = 50 \text{ m}$ with $v = 5 \text{ m/s}$ and 30% relative humidity.

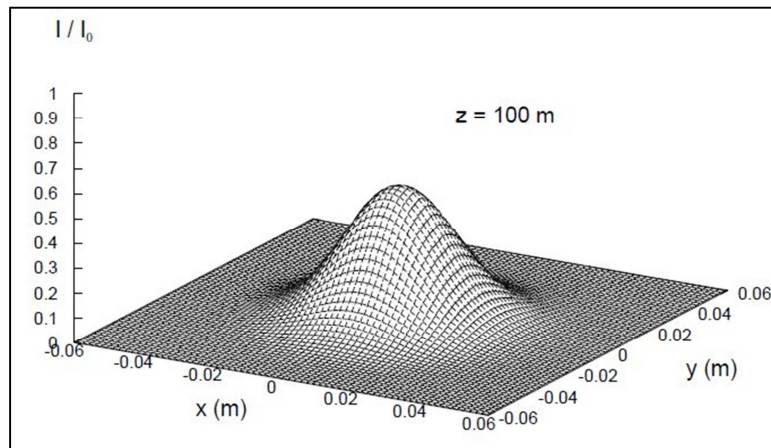


Figure 8. Normalized intensity distribution of laser beam at $z = 100 \text{ m}$ with $v = 5 \text{ m/s}$ and 30% relative humidity.

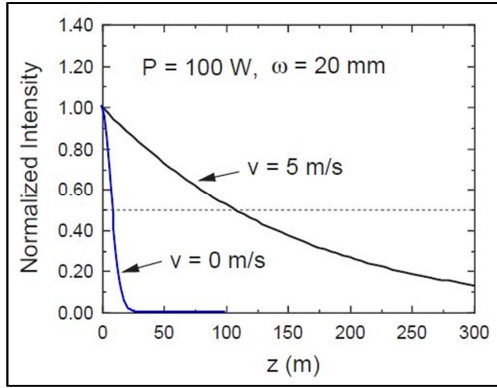


Figure 9. Normalized intensity distributions of laser beams with $P = 100$ W and $\omega = 20$ mm when $v = 0$ and 5 m/s, 30% relative humidity and $\lambda_0 = 1.57\mu\text{m}$.

The intensity distributions of laser beam at $z = 0, 50$, and 100 m were calculated using Eq. (10) when $v = 5$ m/s, $P = 100$ W, $\omega = 20$ mm, 30% relative humidity, and $\lambda_0 = 1.57\mu\text{m}$. The calculated results are shown in Figures 6-8.

As shown in Figures 7 and 8, the beam intensity decreases with increasing z without damaging the initial beam shape. At $z = 100$ m, the intensity of laser beam is about half of the initial intensity at $z = 0$ m.

When $x = y = 0$, the normalized intensity distributions of laser beam with $P = 100$ W and $\omega = 20$ mm were calculated using Eq. (10) when $v = 5$ m/s, 30% relative humidity, and $\lambda_0 = 1.57\mu\text{m}$. The calculated results are shown in Figure 9. For reference, this figure also shows the calculation results when $v = 0$ m/s.

As shown in Figure 9, the $z_h (= 105$ m) when $v = 5$ m/s is about 13 times longer than that ($= 8$ m) when $v = 0$ m/s.

When a lattice-matched InGaAsP/InP is used as an O/E converter for 1.57 μm laser beams, a maximum O/E conversion efficiency (about 45%) was achieved at an incident laser power density of about 1 kW/m² and above [10-12].

If $P = 100$ W and $\omega = 20$ mm is assumed, an incident laser power density of about 1 kW/m² and above is achieved when the normalized intensity I / I_0 is larger than 0.0126.

This minimum I / I_0 (0.0126) is realized at $z \sim 610$ m when $v = 5$ m/s, 30% relative humidity, and $\lambda_0 = 1.57\mu\text{m}$.

The intensity distribution of laser beam at $z = 610$ m were calculated using Eq. (10) when $v = 5$ m/s, $P = 100$ W, $\omega = 20$ mm, 30% relative humidity, and $\lambda_0 = 1.57\mu\text{m}$. The calculated result is shown in Figure 10.

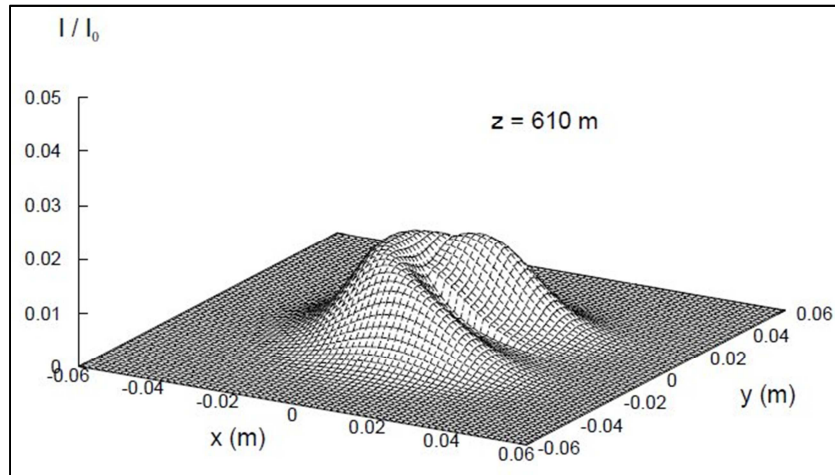


Figure 10. Normalized intensity distribution of laser beam at $z = 610$ m with $v = 5$ m/s and 30% relative humidity.

As shown in Figure 10, the laser beam is shifted into the direction of the flow and the distorted crescent shape of the laser beam appears. This is a self-induced thermal lens effect caused by thermal distortion of laser beam [52].

Thus, under conditions of $v = 5$ m/s and 30% relative humidity, laser beams with $P = 100$ W and $\omega = 20$ mm can propagate over 100 m without damaging the initial beam shape at $\lambda_0 = 1.57\mu\text{m}$.

4. Conclusion

Atmospheric propagation of eye-safe wavelength (1.57 μm) laser beams is affected by the presence of water vapor and aerosols which absorb and scatter the laser energy. The

scattering coefficients of water molecules and aerosols were estimated at wavelength (λ_0) of 1.57 μm . Furthermore, the absorption coefficients of moist air at 30% relative humidity and aerosols were estimated to be about 6.16×10^{-3} and 2.52×10^{-5} m⁻¹, respectively, at $\lambda_0 = 1.57\mu\text{m}$. Then laser beam propagation in the moist atmosphere at $\lambda_0 = 1.57\mu\text{m}$ was theoretically investigated using these coefficients. Under the condition of no wind, the beam intensity decreases rapidly with increasing the length z and the rate of decrease slows down as the beam radius (ω) increases. When z_h is defined as the z where the normalized intensity is halved, the $z_h (= 25$ m) at $\omega = 20$ mm when input power $P = 10$ W is about three times longer than that ($= 8$ m) when $P = 100$ W. This result indicates that the thermal distortion of laser beams due to accumulated

heat around the z axis becomes more conspicuous as the optical power increases. The effect of this thermal beam distortion can be weakened when the laser beam is subject to crosswinds. Under the condition of gentle uniform wind with wind velocity $v = 5$ m/s, propagation of laser beams with $\omega = 20$ mm was studied when $P = 100$ W. The z_h ($= 105$ m) when $v = 5$ m/s is about 13 times longer than that ($= 8$ m) when $v = 0$ m/s. Thus, under conditions of $v = 5$ m/s and 30% relative humidity, laser beams with $P = 100$ W and $\omega = 20$ mm can propagate over 100 m without damaging the initial beam shape at $\lambda_0 = 1.57\mu\text{m}$.

The eye-safe wavelength of $1.57\mu\text{m}$ is very close to the lowest loss wavelength ($1.55\mu\text{m}$) of optical fibers. For this reason, the optical power generated from the light source at $1.57\mu\text{m}$ can be carried through the optical fiber with almost no loss. So it is possible to bring the optical power close to the target through the optical fiber and then emit the light beam toward the target from there.

It is a great advantage of using a light source with an eye-safe wavelength of $1.57\mu\text{m}$ that an optical wireless power transmission system can be constructed flexibly by incorporating optical fiber in some suitable section.

References

- [1] Sumi F. H., Dutta L., and Sarker F. (2018). Future with wireless power transfer technology. *J. Electrical Electronic Sys*, 7 (4), 1000279.
- [2] Zhao M. and Miyamoto T. (2022). Optimization for compact and high output LED-based optical wireless power transmission system. *Photon.*, 9, 14.
- [3] Miyamoto T. (2018). Optical wireless power transmission using VCSELs. *Proc. Soc. Photo-Opt. Instrum. Eng.*, 10682, 1068204.
- [4] Hirota M., Iio S., Ohta Y., Niwa Y., and Miyamoto T. (2015). Wireless power transmission between a NIR VCSEL array and silicon solar cells. 20th Microoptics Conf. (MOC'15), H86.
- [5] Katsuta Y. and Miyamoto T. (2018). Design and experimental characterization of optical wireless power transmission using GaAs solar cell and series-connected high-power vertical cavity surface emitting laser array. *Japn. J. Appl. Phys.*, 57, 08PD01-1-08DP01-7.
- [6] Katsuta Y. and Miyamoto T. (2019). Design, simulation and characterization of fly-eye lens system for optical wireless power transmission. *J. Appl. Phys.*, 58, SJJE02-1-SJJE02-8.
- [7] International Electrotechnical Commission. (2007). IEC 60825 Safety of laser products-Part 1: Equipment classification and requirements. 2nd Edition.
- [8] Duncan K. (2016). Laser based power transmission: component selection and laser hazard analysis. *Proc. IEEE PELS Workshop on Emerging Technologies: Wireless Power Transfer (WoW)*, 2016, 100-103.
- [9] Sahai A. and Graham D. (2011). Optical wireless power transmission at long wavelengths. *Int. Conf. Space Optical Systems Applications (ICSOS 2011)*, 2011, 164-170.
- [10] Mukherjee J., Wulfken W., Hartje H., Steinsiek F., Perren M., and Sweeney S. J. (2013). Demonstration of eye-safe (1550 nm) terrestrial laser power beaming at 30 m and subsequent conversion into electrical power using dedicated photovoltaics. 39th Photovoltaic Specialists Conf. (PVSC 2013), 1074-1076.
- [11] Mukherjee J., Jarvis S., Perren M., and Sweeney S. J. (2013). Efficiency limits of laser power converters for optical power transfer applications. *J. Phys. D*, 46, 264006.
- [12] Jarvis S., Mukherjee J., Perren M., and Sweeney S. J. (2014). Development and characterisation of laser power converters for optical power transfer applications. *IET Optoelectron.*, 8 (2), 64-70.
- [13] Minelly J. D., Barnes W. L., Laming R. I., Morkel P. R., Townsend J. E., Grubb S. G., and Payne D. N. (1993). Diode-array pumping of $\text{Er}^{3+} / \text{Yb}^{3+}$ co-doped fiber lasers and amplifiers. *IEEE Photon. Technol. Lett.*, 5 (3), 301-303.
- [14] Vienne G. G., Caplen J. E., Dong L., Minelly J. D., Nilsson J., and Payne D. N. (1998). Fabrication and characterization of $\text{Yb}^{3+} : \text{Er}^{3+}$ phosphosilicate fibers for lasers. *J. Lightwave Technol.*, 16 (11), 1990-2001.
- [15] Cheo P. K. and King G. G. (2001). Clad-pumped Yb: Er codoped fiber lasers. *IEEE Photon. Technol. Lett.*, 13 (3), 188-190.
- [16] Nilsson J., Alam S.-U., Alvarez-Chavez J. A., Turner P. W., Clarkson W. A., and Grudinin A. B. (2003). High-power and tunable operation of erbium-ytterbium co-doped cladding-pumped fiber lasers. *IEEE J. Quantum Electron.*, 39 (8), 987-994.
- [17] Sahu J. K., Jeong Y., Richardson D. J., and Nilsson J. (2003). A 103 W erbium-ytterbium co-doped large-core fiber laser. *Opt. Commun.*, 227, 159-163.
- [18] Nilsson J., Clarkson W. A., Selvas R., Sahu J. K., Turner P. W., Alam S.-U., and Grudinin A. B. (2004). High-power wavelength-tunable cladding-pumped rare-earth-doped silica fiber lasers. *Optical Fiber Technol.*, 10, 5-30.
- [19] Laroche M., Jander P., Clarkson W. A., Sahu J. K., Nilsson J., and Jeong Y. (2004). High power cladding-pumped tunable Er, Yb-doped fibre laser. *Electron. Lett.*, 40 (14), 855-856.
- [20] Jeong Y., Alegria C., Sahu J. K., Fu L., Ibsen M., Codemard C., Mokhtar M. R., and Nilsson J. (2004). A 43-W C-band tunable narrow-linewidth erbium-ytterbium codoped large-core fiber laser. *IEEE Photon. Technol. Lett.*, 16 (3), 756-758.
- [21] Shen D. Y., Sahu J. K., and Clarkson W. A. (2005). Highly efficient Er, Yb-doped fiber laser with 188 W free-running and > 100 W tunable output power. *Opt. Express*, 13 (13), 4916-4921.
- [22] Laroche M., Girard S., Sahu J. K., Clarkson W. A., and Nilsson J. (2006). Accurate efficiency evaluation of energy-transfer processes in phosphosilicate Er^{3+} - Yb^{3+} -codoped fibers. *J. Opt. Soc. Am. B*, 23 (2), 195-202.
- [23] Jeong Y., Yoo S., Codemard C. A., Nilsson J., Sahu J. K., Payne D. N., Horley R., Turner P. W., Hickey L., Harker A., Lovelady M., and Piper A. (2007). Erbium: ytterbium codoped large-core fibre laser with 297-W continuous-wave output power. *IEEE J. Selected Topics Quantum Electron.*, 13 (3), 573-579.

- [24] Barnhardt E. A. and Streete J. L. (1970). A method for predicting atmospheric aerosol scattering coefficients in the infrared. *Appl. Opt.*, 9 (6), 1337-1344.
- [25] Gebhardt F. (1976). High power laser propagation. *Appl. Opt.*, 15 (6), 1479-1493.
- [26] Knestrick G. L., Cosden T. H., and Curcio J. A. (1962). Atmospheric scattering coefficients in the visible and infrared regions. *J. Opt. Soc. Am.*, 52 (9), 1010-1016.
- [27] Curcio J. A. (1961). Evaluation of atmospheric aerosol particle size distribution from scattering measurements in the visible and infrared. *J. Opt. Soc. Am.*, 51 (5), 548-551.
- [28] Yamamoto G. and Tanaka M. (1969). Determination of aerosol size distribution from spectral attenuation measurements. *Appl. Opt.*, 8 (2), 447-453.
- [29] van de Hulst H. C. (1957). *Light Scattering by Small Particles*. Chap. 20, John Wiley & Sons, New York.
- [30] McClatchey R. A. and Selby J. E. A. (1974). Atmospheric Attenuation of Laser Radiation from 0.76 to 31.25 μm (Environmental Research Paper 460). Air Force Cambridge Research Laboratories, Cambridge.
- [31] Curcio J. A. and Petty C. C. (1951). The near infrared absorption spectrum of liquid water. *J. Opt. Soc. Am.*, 41 (5), 302-304.
- [32] Hale G. M. and Querry M. R. (1973). Optical constants of water in the 200-nm to 200- μm wavelength region. *Appl. Opt.*, 12 (3), 555-563.
- [33] Shuto Y. (2022). High-power laser beam propagation in slightly wet atmosphere. *J. Electrical Electronic Eng.*, 10 (6), 215-222.
- [34] Shoji M. (1995). *Heat Transfer Textbook*. Appendix F, University of Tokyo Press, Tokyo.
- [35] Moosmüller H., Chakrabarty R. K., and Arnott W. P. (2009). Aerosol light absorption and its measurement: A review. *J. Quantitative Spectroscopy Radiative Transfer*, 110, 844-878.
- [36] Bond T. C. and Bergstrom R. W. (2006). Light absorption by carbonaceous particles: An investigative review. *Aerosol Science Technol.*, 40, 27-67.
- [37] Schnaiter M., Horvath H., Möhler O., Naumann K.-H., Saathoff H., and Schöck O. W. (2003). UV-VIS-NIR spectral optical properties of soot and soot-containing aerosols. *Aerosol Science*, 34, 1421-1444.
- [38] Weingartner E., Saathoff H., Schnaiter M., Streit N., Bitnar B., and Baltensperger U. (2003). Absorption of light by soot particles: determination of the absorption coefficient by means of aethalometers. *Aerosol Science*, 34, 1445-1463.
- [39] Zhao G., Yu Y., Yian P., Li J., Guo S., and Zhao C. (2020). Evaluation and correction of the ambient particle spectral light absorption measured using a filter-based aethalometer. *Aerosol Air Quality Research*, 20, 1833-1841.
- [40] Wu Y., Cheng T., and Zheng L. (2020). Light absorption of black carbon aerosols strongly influenced by particle morphology distribution. *Environ. Research Lett.*, 15, 094051.
- [41] Alexander D. T. L., Crozier P. A., and Anderson J. R. (2008). Brown carbon spheres in east asian outflow and their optical properties. *Science*, 321, 833-836.
- [42] Andreae M. O. and Gelencsér A. (2006). Black carbon or brown carbon? The nature of light-absorbing carbonaceous aerosols. *Atmos. Chem. Phys.*, 6, 3131-3148.
- [43] Clarke A. D. and Charlson R. J. (1985). Radiative properties of the background aerosol: Absorption component of extinction. *Science*, 229, 263-265.
- [44] Zender C. S., Bian H., and Newman D. (2003). Mineral dust entrainment and deposition (DEAD) model: Description and 1990s dust climatology. *J. Geophys. Research*, 108 (D14), 4416.
- [45] Ohta S. and Okita T. (1990). A chemical characterization of atmospheric aerosol in Sapporo. *Atmos. Environ.*, 24A (4), 815-822.
- [46] Lukács H., Gelencsér A., Hammer S., Puxbaum H., Pio C., Legrand M., Kasper-Giebl A., Handler M., Limbeck A., Simpson D., and Preunkert S. (2007). Seasonal trends and possible sources of brown carbon based on 2-year aerosol measurements at six sites in Europe. *J. Geophys. Research*, 112, D23S18.
- [47] Kadowaki S. (1979). Silicon and aluminum in urban aerosols for characterization of atmospheric soil particles in the Nagoya area. *Environ. Science Technol.*, 13 (9), 1130-1134.
- [48] Ångström A. (1929). On the atmospheric transmission of sun radiation and on dust in the air. *J. Opt. Geogr. Ann.*, 11, 156-166.
- [49] Smith D. C. (1977). High-power laser propagation: thermal blooming. *Proc. IEEE*, 65 (12), 1969-1714.
- [50] Smith D. C. (1969). Thermal defocusing of CO₂ laser radiation in gases. *IEEE J. Quantum Electron.*, QE-5 (12), 600-607.
- [51] Gebhardt F. G. and Smith D. C. (1969). Effects of wind on thermal defocusing of CO₂ laser radiation. *Appl. Phys. Lett.*, 14 (2), 52-54.
- [52] Gebhardt F. G. and Smith D. C. (1971). Self-induced thermal distortion in the near field for a laser beam in a moving medium. *IEEE J. Quantum Electron.*, QE-7 (2), 63-73.